Simulation and Quantitative Interpretation of Electron Spectra for Surface Analysis

W. S.M. Werner

Institut für Allgemeine Physik, Vienna University of Technology, Wiedner Hauptstraβe 8-10, A 1040 Vienna, Austria

Received 4 October 2004; Accepted 25 January 2005

Quantitative interpretation of electron spectra requires a thorough understanding of the surface sensitivity of the technique, or, in other words, the transfer of the signal electrons from the source to the detector. The theory of electron transport of relevance for XPS, AES, REELS, EPES and related techniques is meanwhile well established. Within the framework of the partial intensity approach it is possible to quantitatively account for elastic scattering of the probing particles by the ionic subsystem as well as volume, surface and intrinsic excitations of the electronic subsystem of the solid. Quantitative spectrum interpretation is achieved by means of Partial Intensity Analysis (PIA) that can be used i.a. to separate the contributions of n-fold inelastically scattered electrons from an experimental spectrum. In particular, it can be employed to eliminate the contribution of multiple scattering from an electron spectrum, ultimately giving the zero-order partial spectrum corresponding to the no-loss peak (a procedure for historical reasons often referred to as background subtraction). The various excitations processes involved in the signal electron escape such as surface, volume and intrinsic excitations are uncorrelated for medium energies. This makes it possible to successively separate contributions corresponding to different types of excitations. In this way, information on the specimen structure is not only conveyed through the signal electron emission process itself, but also through the events taking place along the way between signal electron generation and detection. The relevant procedures are summarized and recent applications are presented. Examples of applications are given in the field of XPS for different surface morphology, total reflection XPS (TRXPS), Auger Photoelectron Coincidence Spectroscopy (APECS), Reflection Electron Energy Loss Spectroscopy (REELS) and Elastic Peak Electron Spectroscopy (EPES).

INTRODUCTION

Quantitative interpretation of electron spectra for surface analysis requires a detailed understanding of the surface sensitivity of electron beam techniques. This is of great relevance for surface analysis techniques such as X-ray photoelectron spectroscopy (XPS), Auger electron spectroscopy (AES), reflection electron energy loss spectroscopy (REELS), elastic peak electron spectroscopy (EPES), Auger photoelectron coincidence spectroscopy (APECS), total reflection XPS (TRXPS) and the like. The superior surface sensitivity of these techniques stems from the strong electron solid interaction [1]. In the present paper, the basic ingredients of the theory for the surface sensitivity are summarized. In this connection the question how the emerging energy and angular signal electron spectrum is related to the energy, angular and depth distribution of the sources must be answered. In other words, the transfer of the signal electrons from their point of generation to emission from the surface is of main concern and is discussed in section 2.

It turns out that the general formula describing the electron transfer can be expressed in terms of fluctuations of the electrons' direction and energy in the course of a given number of interactions on one hand and the probability for a given number of interactions to occur on the other hand. The probability for n_i-fold inelastic scattering is given by the so-called partial intensities, that depend on the boundary conditions of the considered problem. A very efficient procedure to calculate the partial

intensities for electron spectroscopy is the so-called trajectory reversal Monte Carlo algorithm. This algorithm was originally proposed for emission problems about a decade ago [2] and has been successfully employed since that time [3]. It was believed that it can not be applied to reflection problems until recently [4] the corresponding algorithm was found. The trajectory reversal algorithm for calculation of the partial intensities for emission (AES, XPS, APECS) as well as reflection (EPES, REELS) problems is presented in section 3.

In section 4 the formalism for the electron transfer is brought into a form suitable for solving the more difficult and, from the point of view of practical application, more interesting inverse problem, to obtain information on the source energy and depth distribution of a given chemical species on the basis of a measured experimental spectrum. This gives rise to two procedures for spectrum decomposition. The first procedure [5] allows one to eliminate from a measured spectrum the contribution of electrons that have experienced multiple inelastic scattering of a given kind. The second procedure [6] can be used to obtain information on the distribution of energy losses in an individual inelastic excitation of a given type.

Finally, in section 5, several applications of the outlined approaches are given. These include the simulation of elastic peak intensities in EPES, spectrum decomposition of REELS and XPS spectra, the energy distribution in TRXPS and selecting the surface sensitivity with APECS.

THEORETICAL

The starting point for a quantitative theory to describe an electron spectrum for surface analysis is the trivial observation that each electron emitted from the surface has experienced a certain number, say n_i, inelastic collisions n_i=0, 1, 2... Reversing this statement, we conceive the spectrum to consist of groups of n_i-fold inelastically scattered electrons. Since energy losses and deflections as well as the angular and energy distribution of the source function are uncorrelated [1], it follows that the contribution to the spectrum corresponding to the group of n-fold inelastically scattered electrons can be written as a product of an energy dependent function $F_{ni}(E)$, the n_i-th order partial energy distribution, and a function depending only on the emission direction, the partial intensities $C_{ni}(\mu)$. Here $\mu=\cos\theta$ is the off-normal polar emission direction. Choosing the partial energy distributions to be normalized, $\int F_{ni}(E)dE\equiv 1$ implies that these quantities represent the number of particles within the n_i-th group, hence the name. The total spectrum $Y(E,\mu)$ is a superposition of the partial spectra associated with all groups:

$$Y(E,\mu)=\sum_{n_i=0}^{\infty} C_{n_i}(\mu)\Gamma_{n_i}(T)\otimes f_0(E+T) \qquad (1)$$

where $f_0(E)$ is the energy distribution at the source and the symbol ⊗ denotes a convolution. The energy loss T of an electron that has been scattered n_i times is subject to fluctuations, described by the quantities $\Gamma_{ni}(T)$ that are given in terms of an (n_i-1)-fold self-convolution of the distribution of energy losses in an individual energy loss process [1], the normalized differential mean free path for scattering $w_i(T)$:

$$\begin{aligned}\Gamma_0(T)&=\delta(T)\\ \Gamma_{n_i}(T)&=\int_{-\infty}^{\infty}\Gamma_{n_i-1}(T-T')w_i(T')dT'\end{aligned} \qquad (2)$$

The quantities $C_{ni}(\mu)$ represent the number of electrons that arrive in the detector after participating in n_i inelastic collisions and can be established numerically, as described in the next section. The theoretical starting point for the calculation is the distribution $Q(s,\mu)$ of pathlengths s the electron travels inside the solid before reaching the detector. Multiplying this quantity with the probability $W_{ni}(s)$ for experiencing n_i collisions after traveling the considered pathlength gives the partial intensities as an integral over the traveled pathlength:

$$C_{n_i}(\mu)=\int_0^{\infty} Q(s,\mu)W_{n_i}(s)ds \qquad (3)$$

where the collision number distribution $W_{ni}(s)$ in the quasi-elastic energy regime is given by [7]:

$$W_{n_i}(s)=\frac{e^{-s/\lambda_i}}{n_i!}\left(\frac{s}{\lambda_i}\right)^{n_i} \qquad (4)$$

and λ_i is the inelastic mean free path (IMFP). Equation (3) is most useful for calculating the partial intensities for reflection problems as in EPES or REELS. For emission problems, such as AES, XPS, APECS and the like, it is sometimes more convenient to express the partial intensities as an integral over

the depth:

$$C_{n_i}(\mu) = \int_0^\infty \phi_{n_i}(z,\mu) c_0(z) dz \qquad (5)$$

where $c_0(z)$ is the depth distribution of the emitting species and the depth distribution functions $\phi_{ni}(z,\mu)$ describe the probability for escape in the polar emission direction μ for an electron that was generated at the depth z and experienced n_i inelastic collisions on its' way to the surface. Note that the depth distribution functions as defined above represent the integral over the source angular distribution.

If the flux of exciting radiation is inhomogeneous in depth and described by the excitation depth distribution function $\phi_X(z)$, the expression for the partial intensities is transformed into:

$$C_{n_i}(\mu) = \int_0^\infty \phi_{n_i}(z,\mu) \phi_X(z) c_0(z) dz \qquad (6)$$

Finally, it is to be noted that the measured intensity also depends on a number of experimental factors like the analyzer transmission function, the detector efficiency etc. However, for spectrum analysis, the quantities of main importance are the reduced partial intensities γ_{ni}:

$$\gamma_{n_i}(\mu) = c_{n_i}(\mu) / c_{n_i=0}(\mu) \qquad (7)$$

i.e. the partial intensities divided by the area of the no-loss peak. In this case, all experimental factors cancel out.

SPECTRUM SIMULATION

The general theoretical approach outlined in the previous section makes it clear that a spectrum can be simulated by means of the collision expansion in Equation (1). This requires establishing the partial loss distributions that can be easily calculated numerically, either by a direct self-convolution of the differential mean free path, or via a Fast Fourier Transform. Furthermore, the partial intensities need to be calculated. In some special simple cases this can be achieved analytically [1], but in the overwhelming majority of cases it is more convenient to establish these quantities numerically, in particular via a Monte Carlo (MC) simulation.

The MC technique represents a most convenient means to study transport phenomena within the framework of a Boltzmann type kinetic equation where diffraction effects can be disregarded [8]. It is simple to implement and completely flexible with respect to the input parameters and boundary conditions. A disadvantage of this technique is that accumulation of the required statistical accuracy requires considerable computational effort. This is particularly problematic if the solid angle of the detector in the simulation is small, since then a large fraction of the simulated trajectories are generated in vain when they leave the solid in a direction not matching the analyzer acceptance angle (see Figure 1a). In the case of emission problems, this difficulty may be overcome by invoking the symmetry properties of the kinetic equation, the so-called reciprocity relationships for linear transfer [9]. One of these relationships can be interpreted to state that instead of simulating the electron from its' point of emission inside the solid, and following the particles' path until it eventually escapes from the surface in a direction not necessarily matching the analyzer acceptance angle, the trajectory can be generated in reverse, starting in the analyzer from where its' history is traced back in the solid. In this way, it is guaranteed that every simulated trajectory contributes to the calculated signal and the efficiency of the algorithm is drastically improved. By means of this trajectory reversal technique [2, 10, 11], the angular distribution of Auger- or photoelectrons can be rapidly calculated for an arbitrarily small acceptance angle leading to an enhancement in computational efficiency of typically several orders of magnitude. Recently, it has been shown that the trajectory reversal technique can also be applied to reflection problems [4]. The respective algorithms are outlined below.

For *emission* problems, the depth distribution functions can be generated with a trajectory reversal MC simulation [2, 12] from which the partial intensities can be calculated by integration using Equation (6). Alternatively, the partial intensities can be directly generated during the simulation. The latter approach will be described below. The actual simulation of a trajectory is done in the conventional way by sampling the distribution of steplengths, scattering angles etc. and is described in various instances in the literature (see e.g. Ref. [1]). For the

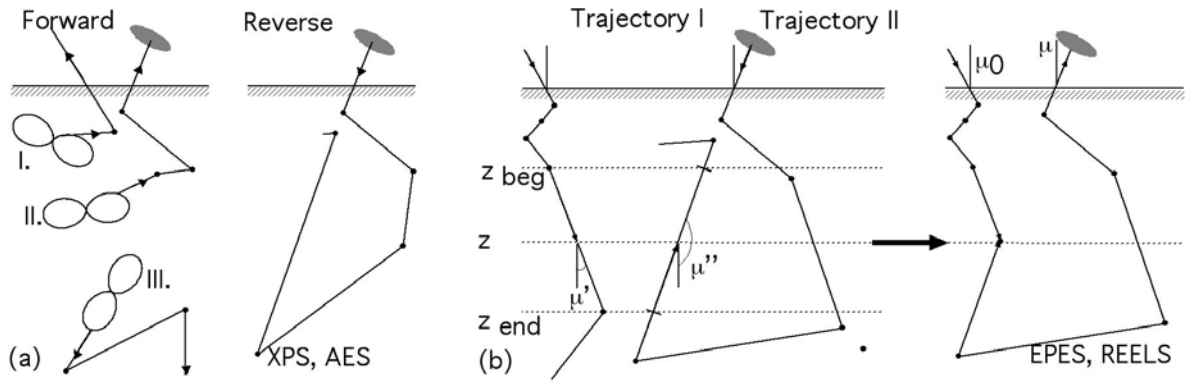

Fig. 1: Illustration of the principle of trajectory reversal. (a.) For emission problems, as in AES and XPS. The left panel shows the forward trajectory approach. Note that trajectories of type I. and III. do not enter the analyzer and are generated in vain. The right panel shows a reverse trajectory that is started in the analyzer and its' history is traced back in the solid. (b.) Illustration of the generation of trajectory pairs for the trajectory reversal algorithm for reflection problems as in EPES or REELS. The left panel shows the "ingoing" (trajectory I.) and "outgoing" (trajectory II.) part of the trajectory, the right panel shows how this trajectory pair is merged at the depth *z* into a trajectory corresponding to a reflected electron (see text).

trajectory reversal simulation, the essential difference is that the initial location and direction of motion of the trajectory is chosen at the surface in a direction along the analyzer axis (see Fig. 1). The history of the electron is then traced back inside the solid. A trajectory is terminated when its' pathlength becomes too long to give a significant contribution to the signal, or when the particle leaves the solid again. This process is repeated for a large number of trajectories.

Evaluation of this set of trajectories can be done in several different ways. One approach is to simply make a histogram of the traveled pathlengths being representative for the pathlength distribution $Q(s,\mu)$, and using eq. (3) to calculate the partial intensities. Combining eqs. (3) and (5) shows that the emission depth distribution functions can also be established in this way, by multiplying the pathlength distribution with the collision number distribution and integrating over the pathlength. However, the integral over the pathlength in eq. (3) can also be carried out analytically during the generation of a given step between elastic collisions. The contribution $(\Delta C_{ni})_k$ of the k-th step to the n_i-th order partial intensity is given by the following recurrence relationship [1]:

$$\left(\Delta C_{n_i}\right)_k = -\left\{W_{n_i}\left(\xi_k + \Delta\xi_k\right) - W_{n_i}\left(\xi_k\right)\right\} + \left(\Delta C_{n_i-1}\right)_k \qquad (8)$$

where $\xi_k = s_k/\lambda_i$ is the reduced length of the k-th step. In this way, one can also take into account the angular and depth distribution of the sources by weighting the k-th step with the source distribution $g_0(\mu_k,\mu_X)$ at the considered depth:

$$\left(\Delta C_{n_i}\right)_k = \left(\Delta C_{n_i}\right)_k \times g_0\left(\mu_k,\mu_X\right) \times c_0\left(z_k\right) \qquad (9)$$

where μ_k, μ_X and z_k are the polar direction of motion and direction of incidence of the exciting radiation and depth along the k-th step, respectively. After generating a large number of trajectories N_{traj} in this way, the partial intensities are found as:

$$C_{n_i} = \frac{\Delta\Omega}{N_{traj}} \sum_{j=1}^{N_{traj}} \sum_{k=1}^{N_k} \Delta C_{n_i,k,j} \qquad (10)$$

where $\Delta\Omega$ is the solid angle of the analyzer.

For a *reflection* geometry, trajectory pairs are generated (see Figure 1b). One of the trajectories of the pair has an incidence angle corresponding to the direction of the electron gun axis, while the other corresponds to the analyzer direction. The trajectory pair can be combined into a set of reflected trajectories at any depth by multiplication with the probability for the corresponding directional change, given by the elastic scattering cross section. At a particular depth z this results in a trajectory where m elastic processes occur "on the way in" and n_e-m-1 occur "on the way out". For a given trajectory pair, all

possible combined trajectories are established by determining the overlapping step segments for all steps taken by trajectory I. For the considered step shown in Figure 1b this gives a contribution to m=4 for the ingoing and n_e-m-1=4 for the outgoing part of the trajectory. Two additional contributions to the fourth step of the "ingoing" trajectory come from n_e-m-1=1 and n_e-m-1=2 of the "outgoing" trajectory. Thus, each trajectory pair is ultimately combined into an infinite number (at least one for each overlapping depth) of reflected trajectories with different collision orders. For any overlapping segment with scattering order (m,n_e), the contribution to the scattering matrix $\Psi_{m,ne}$ is given by[4]:

$$\Delta\Psi_{m,n_e} = \frac{d\sigma_e}{d\Omega}\left(\bar{\Omega}'\cdot\bar{\Omega}''\right)\frac{\lambda_i}{\lambda_e}\frac{e^{-(\Lambda_1+\Lambda_2)/\Lambda_i}}{|\mu'||\mu''|}\frac{\left[e^{-\alpha\Delta z/\lambda_i}-e^{-\beta\Delta z/\lambda_i}\right]}{\beta-\alpha} \qquad (11)$$

In this expression, $\bar{\Omega}'$ and $\bar{\Omega}''$ are the direction of the step along trajectory I and II respectively, Δz is the length of the overlapping segment and Λ_1 and Λ_2 denote the pathlengths traveled before the considered segment. The parameters α and β depend on the directions of the trajectory pair along the overlapping segment and are given in Table I. Finally the elastic reflection coefficient is evaluated via [4]:

$$\eta_e = \frac{|\mu|\Delta\Omega}{N_{pair}}\sum_{n_e=1}^{\infty}\sum_{m=0}^{n_e-1}\frac{\Psi_{m,n_e}}{n_e} \qquad (12)$$

Table I: Parameters α and β of Equation (11). μ' and μ'' represent the polar emission direction along the considered step of trajectory I and II.

μ'	$\mu'\cdot\mu''$	α	β
≥0	≥0	0	$\frac{1}{\lvert\mu'\rvert}+\frac{1}{\lvert\mu''\rvert}$
≥0	<0	$\frac{1}{\lvert\mu''\rvert}$	$\frac{1}{\lvert\mu'\rvert}$
<0	<0	$\frac{1}{\lvert\mu'\rvert}$	$\frac{1}{\lvert\mu''\rvert}$
<0	≥0	$\frac{1}{\lvert\mu'\rvert}+\frac{1}{\lvert\mu''\rvert}$	0
μ''		$\frac{1}{\lvert\mu'\rvert}$	0

SPECTRUM ANALYSIS

In this section, it is explained how the general formalism outlined above can be used for the analysis of experimental data in relevant fields. Spectrum decomposition can be achieved by two main procedures. The first procedure is used to *eliminate* the contribution of multiple inelastic scattering of a given type from an experimental spectrum, the second procedure is used to *retrieve* the differential mean free path for a given type of scattering from an energy loss spectrum. In both procedures it is assumed that the partial intensities have been established (e.g. with the procedures outlined in the previous section).

When the partial intensities are known, Equation (1) can be interpreted as an equation for the unknown lineshape $f_0(E)$, assuming that the differential mean free path $w_i(T)$ is known, or as an equation for the differential mean free path $w_i(T)$ if the source energy distribution $f_0(E)$ is known. The former problem corresponds to *elimination* of multiple scattering (a procedure for historical reasons often referred to as "background subtraction"), the latter problem corresponds to *retrieval* of the interaction characteristics. The solution of these problems is discussed in several papers [1, 5, 13-15].

The *elimination* of multiple scattering can be achieved by iteratively eliminating single, double and higher order inelastic scattering until the considered energy range is free of multiple scattering effects [1, 5, 14]. Denoting the spectrum from which k-fold scattering has been eliminated by Y_k, this can be achieved using the formula [1, 5, 16]:

$$Y_{k+1}(E,\mu_0) = Y_k(E,\mu_0) - \int Y_k(E+T,\mu_0)\Gamma_{k+1}(T)dT \qquad (13)$$

The coefficients q_k are functions of the reduced bulk partial intensities $\gamma_{ni}=C_{ni}/C_{ni=0}$ given in Table II. The subscripts of the coefficients q_k are the partitions of the natural numbers [17].

A solution of Equation (1) to retrieve the distribution of energy losses in an individual collision $w_i(T)$ can be expressed in terms of the loss spectrum $Y_1^L(T)$, i.e. the spectrum from which the elastic peak has been removed [14]. Denoting the (k-1)-fold self-convolution of the loss spectrum by $Y_k^L(T)$, the single scattering loss distribution $w_i(T)$ is found as:

TABLE II: The first few coefficients q_k (Equation (13)) and u_k (Equation (14)) for spectrum deconvolution.

$q_1=\gamma_1$	$u_1=1/\gamma_1$
$q_2=\gamma_2-q_1q_1$	$u_2=(-\gamma_2)/\gamma_1^3$
$q_3=\gamma_3-q_1q_2-q_1q_1q_1$	$u_3=(2\gamma_2^2-\gamma_1\gamma_3)/\gamma_1^5$
$q_4=\gamma_4-q_1q_3-q_2q_2-q_1q_1q_2-q_1q_1q_1q_1$	$u_4=(-5\gamma_2^3-\gamma_1^2\gamma_4+\gamma_1\gamma_2\gamma_3)/\gamma_1^7$
...	...

$$w_i(T)=\sum_{k=1}^{\infty}u_k Y_k^L(T) \qquad (14)$$

Successive orders of multiple scattering are eliminated term by term in the series Equation (14). The coefficients u_k are again functions of the reduced partial intensities and are determined by the recurrence relations given in Ref. [14]. The first few coefficients are explicitly given in Table II.

The remaining question is how to handle a situation where more than one type of inelastic process is of relevance, for example in a reflection energy loss experiment when both surface (subscript "n_s") and bulk (subscript "n_b") excitations are present (but not necessarily clearly distinguishable) in a spectrum:

$$Y_{REELS}(E,\mu)=\sum_{n_s=0}^{\infty}\sum_{n_b=0}^{\infty}C_{n_b,n_s}(\mu)f_0(E+T) \otimes\Gamma_{n_s,n_b}(T)dT \qquad (15)$$

It turns out that the partial intensities for volume scattering on one hand and surface (and also intrinsic) excitations on the other hand are uncorrelated [6]:

$$C_{n_b,n_s}=C_{n_b}C_{n_b} \qquad (16)$$

This condition is generally fulfilled for different types of inelastic scattering if only one of the scattering types involved takes place in a region of space whose dimensions exceed the elastic mean free path since then the region of space where the other types of scattering take place are crossed along a path that is approximately rectilinear [6, 18, 19]. Furthermore, when the different types of inelastic scattering exhibit no interference effects, one has the identity [1]:

$$\Gamma_{n_b,n_s}=\Gamma_{n_b}\Gamma_{n_b} \qquad (17)$$

Inserting Equation (16) and (17) into eq. (15) gives:

$$Y(E,\mu)=\sum_{n_b=0}^{\infty}C_{n_b}(\mu)f_s(E+T)\otimes\Gamma_{n_b}(T)dT \qquad (18)$$

where the spectrum $f_s(E)$, that is free of bulk excitations, is given by:

$$f_s(E,\mu)=\sum_{n_s=0}^{\infty}C_{n_s}(\mu)f_0(E+T)\otimes\Gamma_{n_s}(T)dT \qquad (19)$$

Since the mathematical structure of these two equations is identical to that of Equation (1), the procedures summarized in eq. (13) and eq. (14) can be used to consecutively decompose a spectrum into its constituents corresponding to a given type of inelastic process.

SELECTED APPLICATIONS

Elastic Peak Electron Spectroscopy (EPES)

Elastic peak electron spectroscopy measures the intensity of the (elastic) peak of electrons that are backreflected without any energy loss. The intensity (area) of the elastic peak is equal to the number of electrons escaping without an energy loss, the zero order partial intensity, and depends only on the elastic scattering cross section and the IMFP. Therefore EPES may be used to calibrate the IMFP. Indeed, a large number of papers report on measurements of this quantity by means of EPES [21-31].

A reliable and efficient theoretical model is needed to relate the IMFP and elastic cross section to the elastic backscattering coefficient. In Figure 2, several such models are compared for electrons of several energies backreflected from a Au surface. The angular distribution is shown in the plane of incidence for an analyzer with a polar opening angle of 4°. The left panels are for normal incidence, the right panels for an incidence angle of 75° with respect to the surface normal.

The models that are compared here are the conventional MC simulation, which is taken as representative for the solution of a Boltzmann type kinetic equation (open circles), the trajectory reversal MC algorithm presented above (filled circles labeled "Alg. I."), which is exactly equivalent to conventional

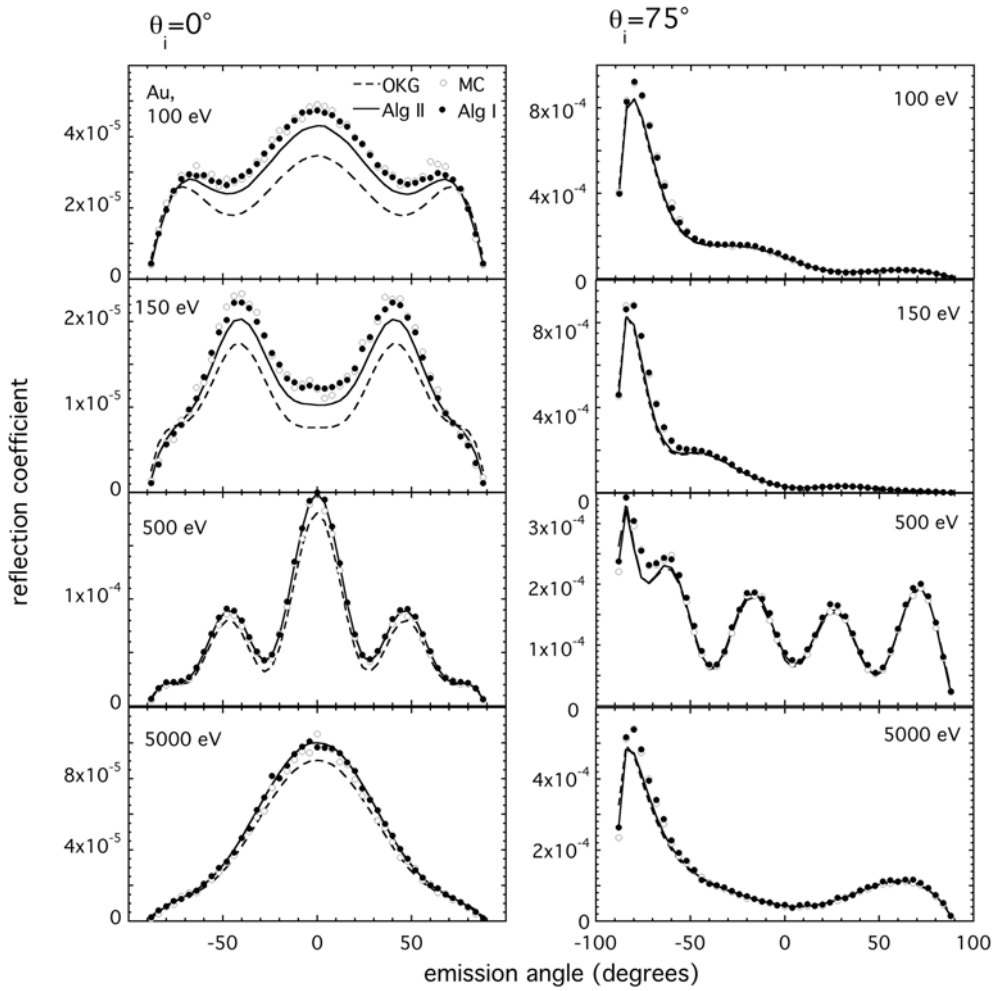

Fig. 2: Differential reflection coefficients for electrons of various energies reflected from a Au surface for normal incidence (left panels) and for an incidence angle of 75° (corresponding to an emission angle of -75° right panels). Open circles: conventional Monte Carlo calculations (MC). Filled circles: trajectory reversal algorithm. Solid lines: approximate trajectory reversal algorithm [4]; Dashed lines Oswald-Kasper-Gaukler model [20].

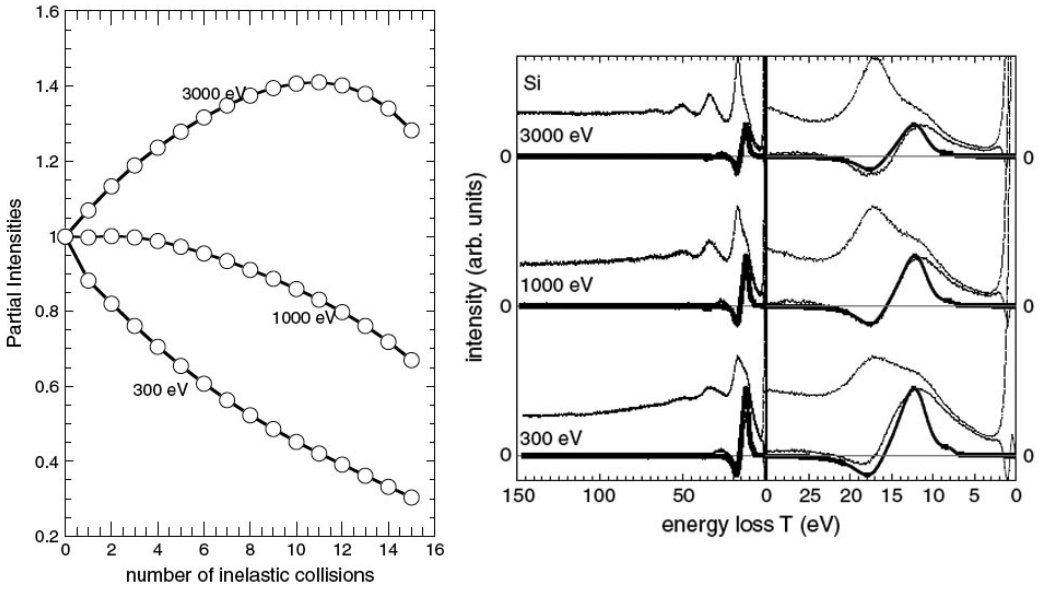

Fig. 3: (a.) Partial intensities for reflection for several energies for a Si target. (b.) The corresponding experimental REELS spectra of Si for several energies. The upper thin lines represent the experimental data. The deconvoluted distribution of energy losses in a single surface excitation are shown as the lower thin lines in each panel. The thick solid lines are the theoretical single surface scattering loss distributions [33]. The right panels show the first 50 eV of the same data in more detail.

MC results, an approximate trajectory reversal algorithm (solid lines labeled "Alg. II") [4] and the Oswald-Kaspar-Gaukler (OKG) model (dashed lines) [20, 32].

It is seen that the conventional MC and the exact trajectory reversal model are in excellent agreement. Note however, that the number of trajectories generated with the trajectory reversal approach was lower by a factor of 1000! When the proper angular correlation at the depth where the trajectory pair is merged is neglected, the approximate trajectory reversal algorithm is obtained. This is even more efficient than the exact one, but is seen to deviate from the exact result for energies below ≲500 eV. When the elongation of the pathlength of the in-and outgoing part of the trajectory is neglected in addition, the OKG model is obtained that can be evaluated analytically but leads to significant deviation of more than 5% in all considered cases.

Reflection Electron Energy Loss Spectroscopy (REELS)

While the intensity of the elastic peak is determined by the zero order partial intensity for a reflection geometry, discussed in the previous section, a REELS spectrum is determined by the higher order partial intensities. As an example, Figure 3 shows the partial intensities for reflection of 300, 1000 and 3000 eV electrons from a Si surface, as well as the corresponding experimental spectra and the spectra deconvoluted with the procedure outlined above (eq. (14)). Note in the survey spectra for Si (left panels of Figure 3b) that the shape of the background over the considered energy range depends significantly on the electron energy: while it is almost perfectly flat for 3000 eV, it decreases with the energy loss for 300 eV. This difference in the shape of the loss distribution is entirely attributable to the details of the elastic scattering process that leads to different shapes of the pathlength distribution [30, 34]. This can be concluded from the data displayed in Figure 3a that present the partial intensities for reflection. These quantities are also seen to be qualitatively different for the different energies. When the proper partial intensities are used in the deconvolution procedure eq. (14), multiple volume scattering is consistently removed from the spectra.

For the low loss region in the Si-spectra, the resulting deconvoluted distribution is seen to consist of a surface plasmon loss at ~11 eV that increases with decreasing energy compared to the bulk plasmon loss at ~17 eV. In the single surface scattering loss

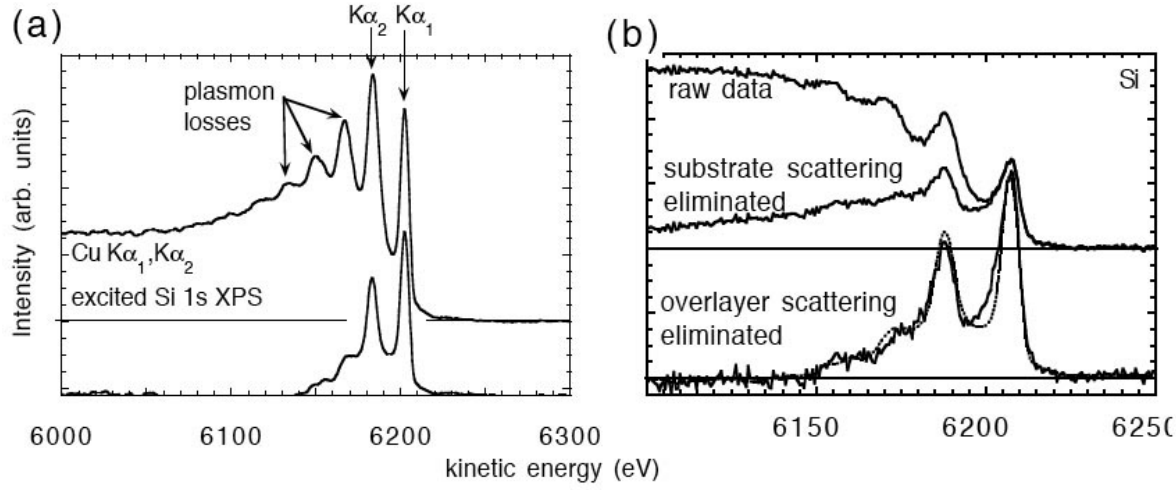

Fig. 4: (a.) Example of application of the background subtraction procedure using Equation (13) to a Cu Kα excited Si spectrum [36]. (b.) Illustration of the general background subtraction procedure applied to the spectrum of a 120 Cu overlayer on a Si substrate. In this case the electron solid interaction was taken into account The dotted line in the lower panel of Figure b is the source energy distribution obtained by applying Equation (13) to the spectrum of a homogeneous Si sample. The two results are seen to be in good agreement.

distribution a negative contribution appears at the position of the bulk plasmon. This is closely matched by the theoretical curve that exhibits a pronounced *begrenzungs* correction at the bulk plasmon energy. The physical origin of this phenomenon is the orthogonality of surface and bulk excitations: the volume modes of the projectile induced field are partly depolarized by the surface charge. The *begrenzungs* effect was predicted by Ritchie almost half a century ago [35], but seems to have never been directly observed before. This emphasizes the necessity of truly quantitative spectrum analysis as explained in the present paper.

X-ray Photoelectron Spectroscopy (XPS)

The true lineshape of a photoelectron peak is important for fundamental studies concerning the chemical environment of the emitting species as well as for quantitative analysis by means of photoelectron spectroscopy. Very often, Tougaards' procedure is used to eliminate the contribution of multiple scattering from electron spectra (for historical reasons commonly referred to as "background subtraction") [37]. However, this procedure only leads to reasonably reliable results in some special simple cases, e.g. when surface excitations can be neglected. In such cases, the partial intensities reduce to a simple mathematical form [1] and the general procedure eq. (13) reduces to Tougaards' approach. When different types of scattering are relevant, the exact sequence of partial intensities becomes important and it is preferable to use eq. (13) with the proper coefficients (as given in Table I).

An example is shown in Figure 4 that shows a high energy XPS spectrum of the Si 1s peak excited with unmonochromatized Cu Kα radiation, giving rise to an apparent doublet peak feature in the spectrum. For such high energies of the emitted signal electrons the signal mainly originates from the bulk of the solid and surface excitations as well as elastic scattering becomes less important compared to lower energies. Elimination of multiple scattering in the bulk by means of eq. (13) results in the spectrum shown in the lower panel.

In Figure 4b the same spectrum is shown after deposition of 120 Å of Cu on the Si substrate. The upper panel also shows the result of elimination of multiple scattering in the substrate, while in the lower panel, overlayer scattering is also eliminated, thereby providing an example of the possibility to subsequently eliminate different types of scattering from the spectrum, as described by eqs. (18) and (19). The dotted line, shown as a reference, is the deconvoluted spectrum shown in Figure 4a, which is

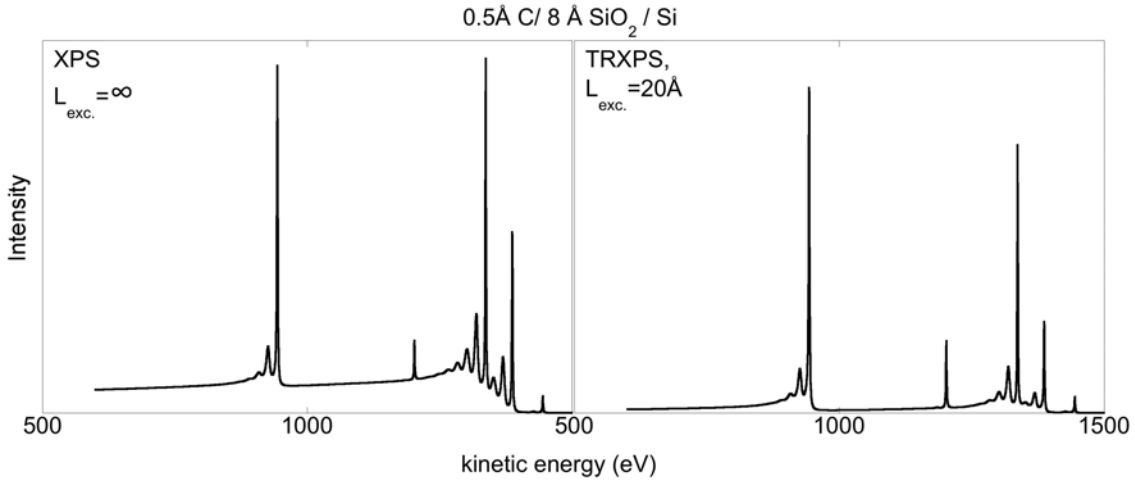

Fig. 5: Simulated spectra of a sample consisting of a 0.5 Å thick C-contamination layer on top of a 10 Å thick SiO_2 layer on a Si-substrate. The left panel shows the simulated ordinary XPS-spectrum, the panel on the right hand side represents the Total Reflection XPS spectrum, when the angle of incidence of the x-rays is close to the angle of total reflection.

in good agreement with the spectrum obtained from the overlayer system. The two shoulders on the low kinetic energy side are attributed to intrinsic excitations [18, 36].

Total Reflection X-ray Photoelectron Spectroscopy (TRXPS)

In ordinary XPS, the angle of incidence of the incoming x-rays is usually far away from the critical angle for total reflection. In this case the length scale over which absorption of the x-rays becomes appreciable is orders of magnitude larger than the inelastic mean free path. The excitation depth distribution function of x-rays striking the surface under a polar angle θ_X can be described in terms of a Beer-Lambert attenuation law:

$$\phi_X(z,\theta_X) = \exp(-m_X \rho z/\cos\theta_X) \qquad (20)$$

where m_X is the mass absorption coefficient determining the relevant excitation range and ρ is the mass density of the material. The characteristic length of the emission depth distribution function is approximately given by the inelastic mean free path that is orders of magnitude smaller $\lambda_i \ll 1/m_X\rho$ for ordinary XPS. In consequence, the excitation depth distribution $\phi_X(z)$ may be assumed to be constant in Equation (6) and the variation of the excitation depth distribution with the depth in the integral (6) can be neglected. Then the surface sensitivity of XPS is entirely determined by the escape process. When the angle of x-rays is close to the critical angle for total reflection $\theta_{X,c}$, the characteristic length for the excitation process becomes comparable to the inelastic mean free path [38] and an angular variation of the (glancing) incidence angle according to eq. (6) allows to probe different depth regions, by effectively changing the excitation depth distribution experimentally.

An example is shown in Figure 5 where simulated spectra [3] are presented for a Silicon substrate covered with an oxide layer of 8 Å thickness and a 0.5 Å thick carbonaceous contamination layer. The left panel shows the Al Kα spectrum for normal incidence of the x-rays, the right panel shows the result corresponding to a incidence geometry close to the critical angle where the excitation length scale is about 20 Å.

Since the excitation depth distribution function decays over a depth range comparable to the zero order emission depth distribution function $\phi_{ni=0}(z,\theta)$, mainly those signal electrons are sampled that escape without being inelastically scattered. In consequence, the higher order partial intensities, that make up the inelastic background, are suppressed since the emission depth distribution function for increasing order of scattering samples increasingly larger depths (approximately $n_i\lambda_i/\cos\theta_e$ for n_i-th order scattering [14]). This explains the reduced inelastic background seen in the TRXPS spectra in Fig. 5.

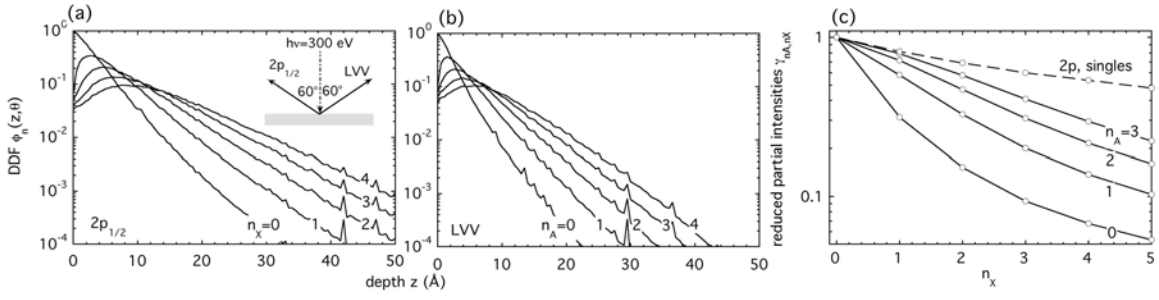

Fig. 6: (a.) Partial escape distribution, or depth distribution function (DDF), $\phi_{nX}(z, \theta_O)$ for the Si $2p_{1/2}$ transition. These data were simulated by means of a Monte Carlo model [3] for normal x-ray incidence and with the Auger and photoelectron detected at an off-normal emission angle of 60° as indicated in the inset. (b) Same as (a), for Si-LVV Auger electrons. (c.) Reduced double differential partial intensities for bulk inelastic scattering $\gamma_{nX,nA}=C_{nX,nA}/C_{nX=0,nA=0}$ calculated from the curves in (a.) and (b.) using Eq (21). The dashed curve represents the Si 2p singles partial intensities for bulk scattering.

Auger Photoelectron Coincidence Spectroscopy (APECS)

In Auger-Photoelectron Spectroscopy (APECS), photoelectrons are measured in coincidence with Auger electrons emitted from the same ionization event. This allows one to study the emission process in greater detail, permitting the identification of initial and final state effects, satellite structures, shake processes etc. [39-45]. In early work in this field [39], it was already pointed out that the surface sensitivity of the technique is enhanced as compared to ordinary electron spectroscopy, manifest in a decreased inelastic background in the experimental spectra [40, 45].

Figures. 6a, b display the escape probability of the Si 2p ($\phi_{n\mathrm{X}}(z)$) and Si-LVV ($\phi_{n\mathrm{A}}(z)$) electrons which have experienced a certain number of volume excitations. It can be seen that the depth ranges sampled by the depth distribution functions for the Si 2p and the Si-LVV peak are distinctly different. In the case of APECS, one is only interested in electrons created at the same location, and the partial intensities for APECS for an ideally flat homogeneous surface can be written as:

$$C_{n_A,n_X} = \int_0^\infty \phi_{n_X}(z)\phi_{n_A}(z)dz \qquad (21)$$

where n_X and n_A denote the collision number of the photo- and Auger electron, respectively. A survey of the collision statistics for the Si 2p APECS core hole spectrum is presented in Figure 6c that displays the partial intensities normalized by the elastic peak area. If the Si 2p peak is measured in coincidence with the LVV no-loss peak (curve labeled n_A=0), the first and higher order plasmons ($n_\mathrm{X}\geq 1$) are strongly reduced with respect to the singles spectrum (dashed line). If the same spectrum is measured in coincidence with the first plasmon in the Auger line (n_A=1), the intensity of the inelastic background increases again. Since the probability for inelastic scattering increases monotonically with the respective pathlength, those Auger electrons that end up in the first plasmon peak originate from larger depths. Then the 2p electrons measured in coincidence with them will also travel a longer pathlength in the solid and the probability for experiencing an inelastic collision increases. The above implies that the emission depth of the elastic peak in the photoelectron spectrum (n_X=0) can be selected by measuring the spectrum in coincidence with energies corresponding to a particular number of plasmon losses in the Auger line. In other words, the surface sensitivity of APECS can be selected by measuring the photoemission line in coincidence with different energies in the inelastic tail of the Auger line and vice versa.

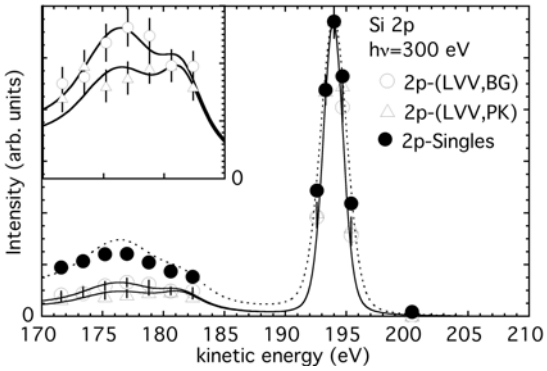

Fig 7: Si-2p spectrum measured in coincidence with the background in the Si-LVV spectrum (open circles),as well as with the peak of the Si-LVV Auger line (open triangles). The filled circles are the corresponding singles intensities. The solid and dotted lines represent results of model calculations with the SESSA-Software (Simulation of Electron Spectra for Surface Analysis) [3] (see text). The inset shows an expanded view of the BG and PK spectra.

An example of the latter statement is shown in Fig. 7 [46]. The filled circles represent the ordinary ("singles") XPS spectrum, the open triangles (labeled "PK") represent the Si 2p peak measured in coincidence with the no-loss feature in the Si-LVV Auger peak while the open circles (labeled "BG") are the spectrum in coincidence with the first plasmon loss in the Auger peak. The three spectra were normalized to the same peak height in the maximum. It is seen that the plasmon in the "PK" spectrum is significantly reduced with respect to the singles spectrum, a manifestation of the enhanced surface sensitivity of APECS [39]. In the BG-spectrum the intensity of the first volume plasmon increases again, indicating that larger depths are sampled in this case. The results are in close agreement with model calculations [3] thereby proving the ability of APECS to discriminate the average emission depth of individual electrons: while the electrons in the PK spectrum originate from an average depth of about 2.0±2.1 Å, the average emission depth of the BG spectrum amounts to about 4.7±4.9 Å. The singles

spectrum, on the other hand, consists of electrons emitted from an average depth of 6.1±6.5 Å. The uncertainties quoted for the emission depths represent the root-mean-square widths $\sigma_{<z>}$ of the fluctuations in the emission depth that are inherent to the stochastic process for multiple scattering [46].

REFERENCES

[1] W. S. M. Werner, Surf. Interface Anal. **31**, 141 (2001).

[2] W. H. Gries and W. S. M. Werner, Surf. Interface Anal. **16**, 149 (1990)

[3] W. S. M. Werner, W. Smekal, and C. J. Powell, Simulation of Electron Spectra for Surface Analysis (National Institute for Standards and Technology (NIST), Gaithersburg (MD), US, 2004).

[4] W. S. M. Werner, Phys. Rev. (2004).

[5] W. S. M. Werner, Phys. Rev. **B52**, 2964 (1995).

[6] W. S. M. Werner, Surf. Sci. **526/3**, L159 (2003).

[7] W. S. M. Werner, Phys. Rev. **B55**, 14925 (1997).

[8] W. Smekal, W. S. M. Werner, C. S. Fadley, and M. A. van Hove, J. Electron Spectrosc. Rel. Phen. **137**, 183 (2004).

[9] K. M. Case and P. F. Zweifel, Linear Transport Theory (Addison-Wesley, Reading, MA, 1967).

[10] I. S. Tilinin and W. S. M. Werner, Phys. Rev. **B46**, 13739 (1992).

[11] W. S. M. Werner, I. S. Tilinin, and A. Jablonski, Surf. Interface Anal. **23**, 823 (1995).

[12] P. Cumpson, Surf. Interface Anal. **20**, 727 (1993).

[13] W. S. M. Werner, in Surface Analysis by Auger and X-Ray Photoelectron Spectroscopy, edited by D. Briggs and J. Grant (IMPublications, Chichester, UK, 2003).

[14] W. S. M. Werner, Surf. Interface Anal. **23**, 737 (1995).

[15] M. Vicanek, Surf. Sci. **440**, 1 (1999).

[16] W. S. M. Werner, T. Cabela, J. Zemek, and P. Jiricek, Sur.f Sci. **470**, 325 (2001).

[17] S. Ahlgren and K. Ono, Notices of the AMS 48, 978 (2001).

[18] W. S. M. Werner and P. Schattschneider, J. Electron Spectrosc. Rel. Phen. (in print) (2004).

[19] W. S. M. Werner, Surf. Interface Anal. **35**, 347 (2003).

[20] R. Oswald, E. Kasper, and K. Gaukler, J. Electron Spectrosc. Rel. Phen. **61**, 251 (1993).

[21] R. Schmid, Ph.D. thesis, University of Tübingen, Germany (1982).

[22] A. Jablonski, B. Lesiak, and G. Gergely, Physica Scripta **39**, 363 (1989).

[23] A. Jablonski, P. Mrozek, G. Gergely, M. Menhyard, and A. Sulyok, Surf. Interface Anal. **6**, 291 (1984).

[24] W. Dolinski, S. Mroz, and M. Zagorski, Surf. Sci. **200**, 361 (1989).

[25] W. Dolinski, H. Nowicki, and S. Mroz, Surf. Interface Anal. **11**, 229 (1989).

[26] H. Beilschmidt, I. S. Tilinin, and W. S. M. Werner, Surf. Interface Anal. **22**, 120 (1994).

[27] Y. F. Chen, J. Vac. Sci. Technol. **A13(6)**, 2665 (1995).

[28] A. Koch, PhD Thesis (University Tübingen, 1996).

[29] C. J. Powell and A. Jab ɪ 0 · onski, J Phys Chem Ref Data 28, 19 (1999).

[30] W. S. M.Werner, C. Tomastik, T. Cabela, G. Richter, and H. Störi, J. Electron Spectrosc. Rel. Phen. **113**,127 (2001).

[31] W. S. M. Werner, C. Tomastik, T. Cabela, G. Richter, and H. Störi, Surf. Sci. **470**, L123 (2001).

[32] R. Oswald, Ph.D. thesis, Eberhard-Karls-Universität Tübingen (1992).

[33] Y. F. Chen, Surf. Sci. **345**, 213 (1996).

[34] W. S. M. Werner and M. Hayek, Surf. Interface Anal. **22**, 79 (1994).

[35] R. H. Ritchie, Phys. Rev. **106**, 874 (1957).

[36] W. S. M. Werner, L. Köver, J. Toth, and D. Varga, J. Electron Spectrosc. Rel. Phen. **122**, 103 (2002).

[37] S. Tougaard and P. Sigmund, Phys. Rev. **B25**, 4452 (1982).

[38] B. L. Henke, Phys. Rev. **A6**, 94 (1972).

[39] H. W. Haak, G. A. Sawatzky, and T. D. Thomas, Phys. Rev. Lett. **41**, 1825 (1978).

[40] C. P. Lund and S. M. Thurgate, Phys. Rev. **B50**, 17166 (1994).

[41] S. M. Thurgate and Z.-. T. Jang, Surf. Sci. **466**, L807 (2000).

[42] S. M. Thurgate, Surf. Interface Anal. **20**, 627 (1993).

[43] E. Jensen, R. A. Bartynski, S. L. Hulbert, and E. D. Johnson, Rev. Sci. Instrum. **63**, 3013 (1992).

[44] E. Jensen, R. A. Bartynski, S. L. Hulbert, E. D. Johnson, and R. Garrett, Phys. Rev. Lett. **62**, 71 (1989).

[45] E. Jensen, R. A. Bartynski, , R. Garrett, S. L. Hulbert, E. D. Johnson, and C. C. Kao, Phys. Rev. **B45**, 13636 (1992).

[46] W. S. M. Werner, W. Smekal, H. Störi, H. Winter, G. Stefani, A. Ruocco, F. Offi, R. Gotter, A. Morgante,and F. Tomasini, Phys. Rev. Lett. **94**, 038302 (2005).